Vibronic effects in the photoelectron spectrum of ozone

(Dated: August 16, 2024)

Abstract

I. INTRODUCTION

Ozone is a C_{2v} molecule with three normal modes: symmetric stretch, symmetric bend, and asymmetric stretch. The asymmetric stretch is of a b_2 symmetry. The two lowest electronic states of the ozone cation are close in energy. The lower state is fully symmetric while the higher one is of the B_2 symmetry, the same symmetry as the asymmetric stretch. The close energetic separation and the matching symmetry of the asymmetric stretch results in significant vibronic effects appearing in the ozone photoelectron spectrum. Figure 1 presents a graphical summary of this information.

II. METHODS

We simulate the vibronic states of the ozone cation using the model Hamiltonian of Köppel, Domcke, and Cederbaum (KDC Hamiltonian).[1–3] This is a multi-state and multi-mode Hamiltonian defined in the basis of diabatic states. We consider the ozone cation in the basis of two quasi-diabatic states coupled by one mode (mode number 3). The model

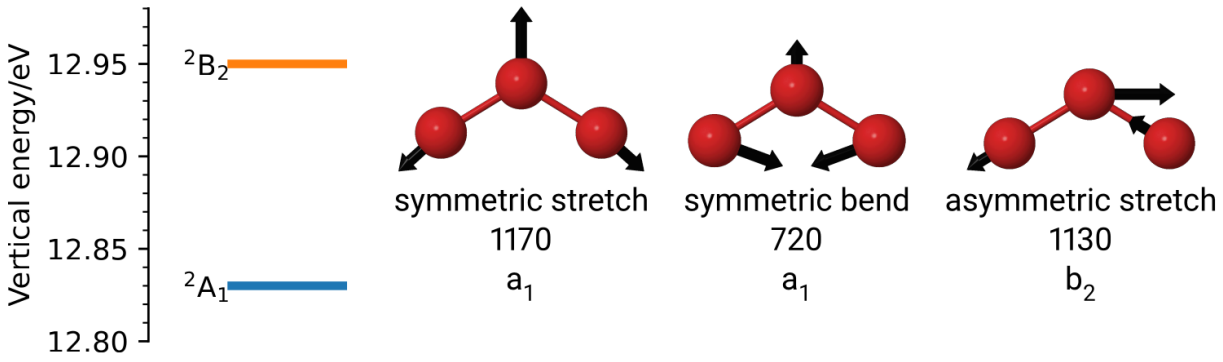

FIG. 1. Two lowest states of the ozone cation and normal modes of ozone.

also includes two symmetric modes (modes number 1 and 2)

$$H = H_0 \mathbf{1} + \begin{pmatrix} V^{(1)} & \lambda_3 Q_3 \\ \lambda_3 Q_3 & V^{(2)} \end{pmatrix} \tag{1a}$$

$$H_0 = \frac{1}{2}\left(\sum_{i=1}^{3} -\omega_i \frac{\partial^2}{\partial Q_i^2}\right) + \frac{1}{2}\omega_3 Q_3^2 \tag{1b}$$

$$V^{(\alpha)} = E^{(\alpha)} + \sum_{i,j,k,l \in \{1,2\}} \kappa_i^{(\alpha)} Q_i + \kappa_{ij}^{(\alpha)} Q_i Q_j + \kappa_{ijk}^{(\alpha)} Q_i Q_j Q_k + \kappa_{ijkl}^{(\alpha)} Q_i Q_j Q_k Q_l. \tag{1c}$$

The Hamiltonian parameters are expanded around the equilibrium geometry of ozone. $E^{(\alpha)}$ are the vertical ionization energies calculated at that geometry. Q_i are the dimensionless normal coordinates of ozone. κ are the coefficients of expansion of the potential along the fully symmetric coordinates. λ are the linear diabatic couplings. ω are the harmonic frequencies of ozone.

We find the parameters that enter the KDC Hamiltonian using *ab inito* coupled-cluster (CC) methods and its equation-of-motion EOM-CC extension.[4–9] We use the CC truncated to singles and doubles (CCSD), singles, doubles and triples (CCSDT) as well as singles, doubles, triples and quadruples (CCSDTQ).[10] We use the EOM-CC for ionization potential (EOM-IP).[11] We use the Ichino, Gauss and Stanton definition of quasi-diabatic states based on the EOM-CC method (EOM-CC-QD)[12]. In all CC and EOM-CC calculations we leave all electrons correlated, in other words, we do not use the frozen-core approximation.

Using CCSDT/ANO1 we optimize the geometry of ozone and compute its harmonic frequencies and normal coordinates.[13,14] At the same geometry we compute the linear diabatic coupling λ using EOM-IP-CCSD-QD/ANO1. We use EOM-IP-CCSDT/ANO1 on a grid to find the expansion coefficients κ.

The vertical ionization energies are calculated using a composite method. The base value is the complete basis set (CBS) extrapolation of the EOM-IP-CCSDT/cc-pCVnZ energies with n = 5, 6.[15] These values are augmented with two corrections: the ΔQ correction in the cc-pwCVTZ basis set and the relativistic correction calculated using EOM-IP-CCSD/cc-pwCVTZ.[16] We introduce an error estimates to the reported vertical energies. For the error estimate of the extrapolated CBS value we use half of the absolute value of the difference between the best *ab initio* value and the extrapolated value. For the remaining corrections we use as the error estimate half of the absolute value of the correction.

TABLE I. Vertical ionization energies with the error estimates, eV.

Contribution	$^2A_1$	$^2B_2$	Error estimate
CBS	12.872	12.981	0.02
ΔQ	-0.037	-0.021	0.02
Relativistic	-0.008	-0.010	0.005
Sum	12.827	12.950	0.03

To compare the simulated photoelectron spectrum to the experimental one, we use the oscillator strengths ratio A_1:B_2 of 1:1.35.[17] Additionally, the stick spectrum is broadened with the Lorenzian envelopes normalized to the peaks' intensities

$$f_{envelope}(x, x_i, I_i) = \frac{I_i}{(x - x_i)^2 + (\gamma/2)^2}. \quad (2)$$

x_i is the position of the spectral peak, I_i is its intensity and γ is the peak's width.

We use the XSIM program of Dr. Stanton to simulate the spectrum using the basis of 50 harmonic states in each mode and 6000 iterations of the Lanczos procedure. All remaining *ab initio* calculations are completed using CFOUR.[18,19]

III. RESULTS

The optimized geometry of ozone gives the bond lengths of 1.270 Å and the bond angle of 116.9°. The two symmetric normal modes have frequencies 1169 cm^{-1} and 724 cm^{-1}, while the asymmetric stretch has frequency equal to 1129 cm^{-1}. The computed value of the linear diabatic coupling constant λ is 1394 cm^{-1}. The vertical ionization energy for the first excited state, $E^{(1)}$, computed using the composite method described above is equal to 12.827 eV. Our error estimate for this value is 30 meV, see Table I for details. We note that the convergence of the vertical ionization gap between the two states is much faster and we estimate this value as equal to 123 ± 8 meV, see Table II for details.

Figure 2 compares the simulated spectrum to the experimental one taken from reference[20]. A comparison of the simulated and experimental spectra is presented on Figure 2 and shows a good match. Peak A is known to be a hot band.[17] The simulation reproduces well the consecutive increase in the intensities of peaks B, C, D, and E. The spacing between these

TABLE II. The energy gap between vertical ionization energies of the $^2A_1$ and $^2B_2$ states with error estimates, meV. See caption of Table I.

Contribution	Gap	Error estimate
EOM-CCSDT/CBS	108.8	0.9
ΔQ/pwCVTZ	16.5	8
Relativistic/CCSD/pwCVTZ	-2.2	1.1
Final value, meV	123	8
Final value, cm^{-1}	990	65

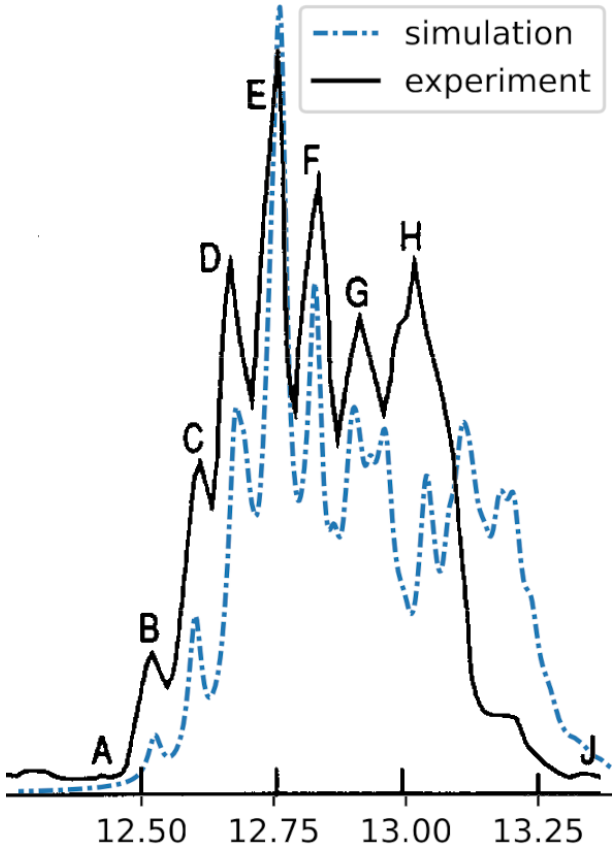

FIG. 2. Comparison of the experimental (solid black line) and the simulated spectrum. In the simulated spectra the plot is generated with peak width $\gamma = 30$ meV. The simulated spectrum is shifted towards higher energies by 21 meV.

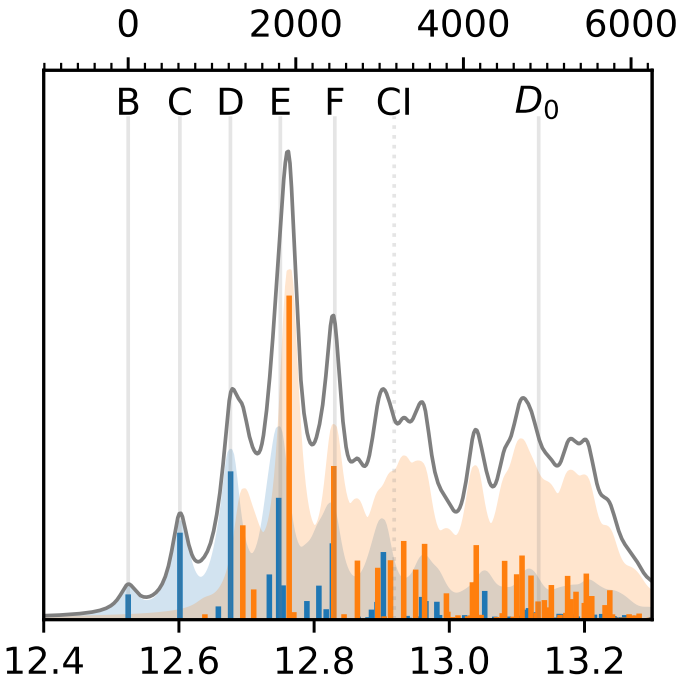

FIG. 3. Simulated photoelectron spectrum of ozone. Bottom axis shows energy scale in eV. Top axis shows energy offset from the origin in cm^{-1}. Stick spectrum shows positions and intensities of all simulated states. Blue color corresponds to the oscillator strength originating from the $^2A_1$ basis state while the red ones correspond to $^2B_2$. Gray vertical lines with captions on top indicate positions of features as measured by the PFI-ZEKE experiment.[21] D_0 marks the dissociation threshold of O_3^+. Gray dotted line marks the energy of the minimum of the conical intersection (CI).

peaks is also well reproduced. Drop in the intensity of peak F is also captured by the simulation. Starting from peak G the simulation shows discrepancy with the experiment. A sudden drop in the intensity past the peak H is not observed in the simulation. We discuss a likely source of this mismatch later.

Our simulation allows for an additional element of analysis of the simulated spectrum. Figure 3 presents the same simulated spectrum as in Figure 2 with additional information on the decomposition of the spectrum. All lines that contribute to the spectrum are marked individually and in two different colors. The spectrum shows that peaks A and B are almost purely of the $^2A_1$ character. Starting from peak C each the contributions from two states are

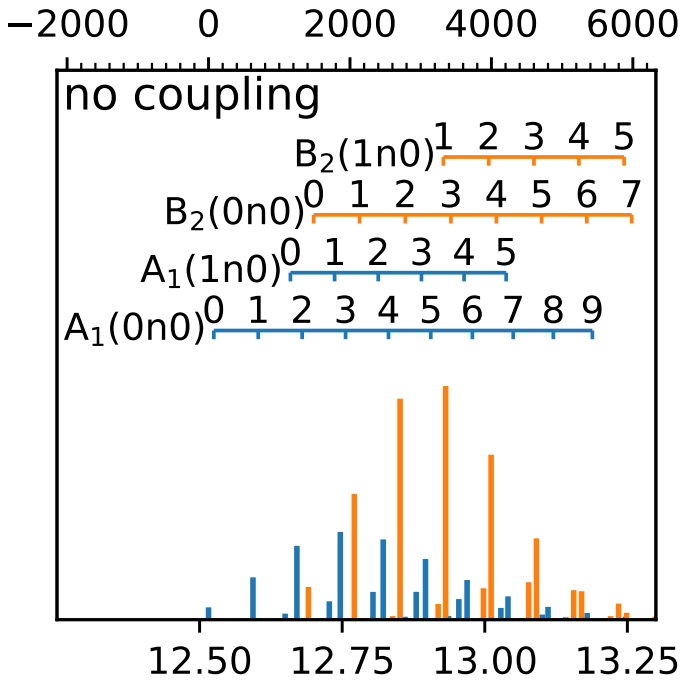

FIG. 4. Simulated photoelectron spectrum of ozone, but with no account given to the vibronic coupling effect.

equally important, it is also clear that each peak of the low-resolution spectrum has in fact contributions from many vibronic peaks. At the energy of about 2000 cm^{-1} above the origin the density of vibronic peaks increases significantly. This value can be compared to the minimum of the conical intersection, which our simulation locates at 3174 cm^{-1} above the origin (12.92 eV). Our simulation is incapable of accounting for dissociation of the molecule, therefore the we expect a discrepancy with the experiment as the energy gets closer to the dissociation threshold located at 4840 cm^{-1} above the origin.[21]

We would like to assign the vibronic peaks from our simulation. To this end, we run the simulation once again, this time, however we set the linear diabatic constant to zero, i.e., $\lambda = 0$. With that change we can reproduce the spectrum (at an equivalent level of theory) but in an artificial case where there is no vibronic coupling. Figure 4 presents this spectrum. The non-coupled spectrum is easy to assign using the labels that mark the symmetry of the electronic state, A_1 or B_2, and the vibrational state ($\nu_1\nu_2\nu_3$), where ν_i is the number of quanta in mode i with $i = 1$ for the symmetric stretch, $i = 2$ for the symmetric bend

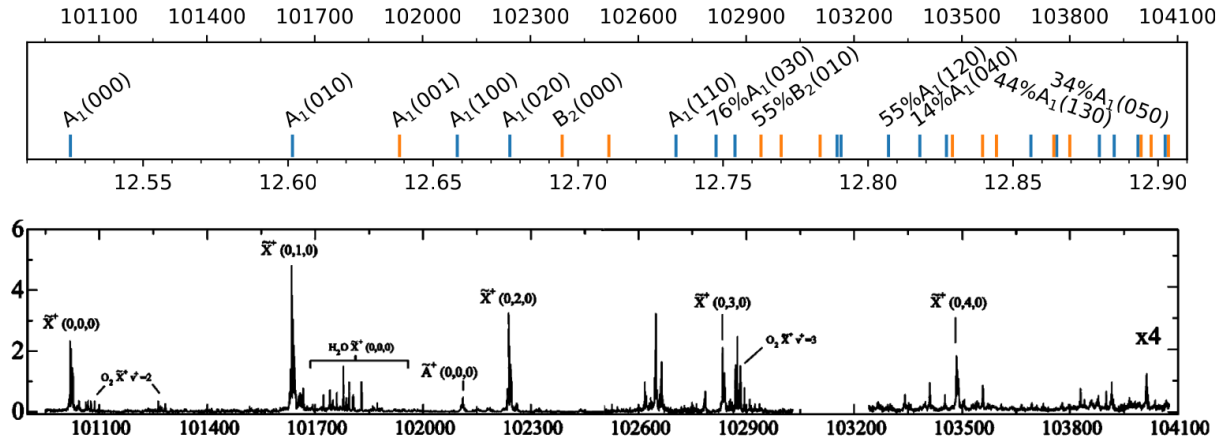

FIG. 5. Comparison of the simulated spectrum with the PFI-ZEKE experiment.[21] The simulated spectrum was shifted by 21 meV= 170 cm^{-1} towards higher energies.

and $i = 3$ for the asymmetric stretch. The assigned spectrum shows progressions in the symmetric bend. There is one such progression in each electronic states. Additionally for each state, there is also another progression in the symmetric bend with one excitation in the symmetric stretch.

We decompose the vibronic states of our main simulation in the basis of the artificial, uncoupled states discussed in the previous paragraph. Figure 5 shows the assigned spectrum and Table III lists the decomposition of all peaks in the region of up to 3000 cm^{-1} with intensities larger than 10^{-3}. We compare the assigned spectrum against the high-resolution pulsed-field-ionization zero-kinetic-energy (PFI-ZEKE) spectrum from 2005.[21] The PFI-ZEKE spectrum is the best source of information on the location of the peaks, especially the origin, against which align our simulation. The origin of the simulated spectrum is located 170 cm^{-1} lower than the experimental origin which was experimentally observed at $101,020.5$ cm^{-1}.[21] This is within our error estimate for the vertical ionization energy (30 meV= 240 cm^{-1}). Once the origin locations are aligned the comparison shows a good match between the simulation and the experiment. Especially the states with an oscillator strength originating from the A_1 state are well aligned with the experimental features.

States close to the origin of the band are similar to the non-coupled states. The origin peak is of a clear $A_1(0,0,0)$ character, the first two excitations in the symmetric bend, $A_1(0,1,0)$ and $A_1(0,2,0)$ are also very similar to the non-coupled states, while the higher

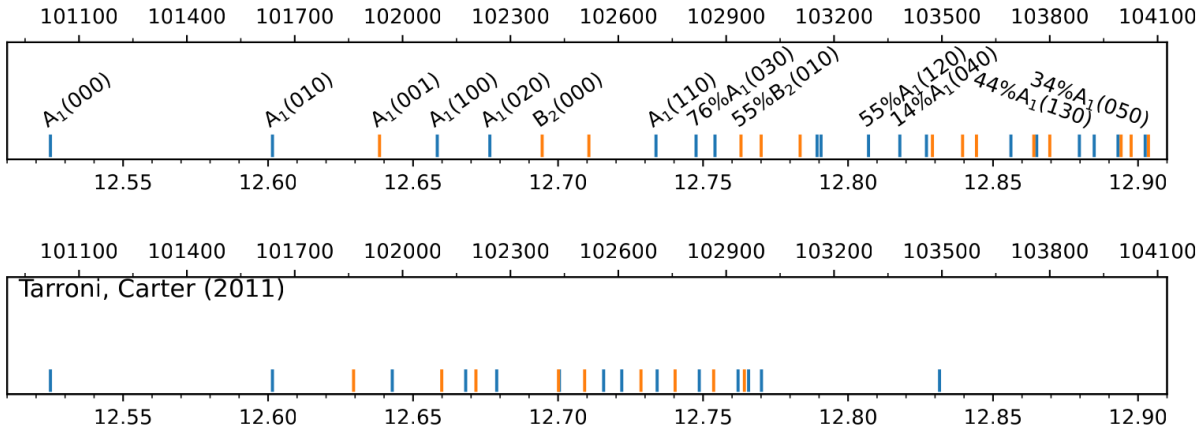

FIG. 6. Comparison of the simulated spectrum to an earlier accurate simulation of Tarroni and Carter (assigned lines).[22]

excitations in this progression are showing large mixing. The same progression with one vibrational quantum in the symmetric stretch is more interesting. The first of its peaks is very well aligned with an experimentally visible feature, which was previously assigned as the origin of the second state. The second peak in this series, the first combination state $A_1(1,1,0)$, has very high similarity to its uncoupled version. It is a good candidate to assign the experimental, unassigned feature above $102,600$ cm^{-1}.

States with an oscillator strength from the B_2 state are on the other hand not aligning well with the experiment. First such peak, close to the 12.64 eV mark on the Figure 5, is of a vibronic character and we assign it as a $A_1(0,0,1)$ state which gains intensity thanks to the coupling to the B_2 state. This vibronic peak lies in the part of the spectrum marked as pollution due to water. The origin of the B_2 state is very similar to the uncoupled $B_2(0,0,0)$ state, but it is located in an empty area of the experimental spectrum. The next peak, slightly above the 12.76 eV mark on Figure 5, corresponds to the one excitation of the symmetric bend in the B_2 state, but as the label on the figure shows, it is only about 55% similar to the uncoupled state.

Finally, we compare our simulation to an earlier accurate simulation, the work of Tarroni and Carter from 2011.[22] Both spectra show a good match to the experiment and agree in the assignment of the first progression in the bending mode. The previous simulation, however, shows smaller spacing between other lines, showing much higher congestion of the spectrum. Additionally the origin of the second state falls at lower energy aligning well with

TABLE III. Assignment and decomposition of the eigenvectors of the ozone cation.

Peak position (cm^{-1})	Assignment	Eigenvector
0	$A_1(000)$	$-0.99\ A_1(000)$
618	$A_1(010)$	$+0.99\ A_1(010)$
915	$A_1(001)$	
1076	$A_1(100)$	$-0.99\ A_1(100)$
1222	$A_1(020)$	$-0.97\ A_1(020)$
1368	$B_2(000)$	$+0.97\ B_2(000)$
1498		$-0.10\ B_2(000)$
1684	$A_1(110)$	$-0.96\ A_1(110)$
1796	$A_1(030)$	$-0.87\ A_1(030) - 0.16\ A_1(110) - 0.13\ A_1(020) + 0.13\ A_1(040)$
1848		$+0.31\ A_1(030)$
1921	$B_2(010)$	$-0.74\ B_2(010) + 0.18\ B_2(020) + 0.11\ B_2(000)$
1977		$+0.24\ B_2(010)$
2085		$-0.52\ B_2(010)$
2132		$+0.25\ A_1(030) + 0.24\ A_1(040) + 0.13\ A_1(120) - 0.13\ A_1(050)$
2275	$A_1(120)$	$+0.86\ A_1(120) + 0.12\ A_1(040)$
2363		$-0.62\ A_1(040) + 0.40\ A_1(120) - 0.17\ A_1(030) + 0.11\ A_1(050)$
2439		$+0.47\ A_1(040) + 0.12\ A_1(120)$
2454		$+0.53\ B_2(020) + 0.24\ B_2(010) - 0.17\ B_2(030)$
2576		$+0.27\ B_2(020)$
2736		$+0.60\ B_2(020)$
2886	$A_1(130)$	$-0.81\ A_1(130) + 0.12\ A_1(050) - 0.10\ A_1(120)$
2974		$-0.24\ B_2(110) - 0.16\ B_2(020)$
3047	$A_1(050)$	$+0.76\ A_1(050) + 0.13\ A_1(130)$

the peak that was assigned in the PFI-ZEKE also as the origin of the second state. While an additional simulation of the line intensities would allow for the most complete comparison to the experimental spectrum, the strong alignment of the simulated peaks of a leading A_1 character with the experimental features leads us to believe that our simulation offers the best assignment of the spectrum to date.

IV. SUMMARY AND CONCLUSIONS

We have simulated the vibronic effects in the photoelectron spectrum of the ozone. We have used the KDC Hamiltonian[1–3] with the *ab initio* parametrisation of the quasi-diabatic

states of Ichino, Gauss and Stanton.[12] The results of our simulation match well the photoelectron spectrum from 1970s[20] and the PFI-ZEKE spectrum from 2005.[21] We present analysis of the spectra and highlight the role of the vibronic coupling effects. Our simulation offers a state-of-the-art insight into the spectrum and allows us to assign the simulated peaks. Our assignment agrees well with the previously assigned progression in the symmetric bend but we reassign some of the other features of the spectrum. Simulated peaks that gain intensity from the B_2 state are absent in the PFI-ZEKE spectrum which offers an interesting avenue for further investigations. Modeling of the intensity of the PFI-ZEKE peaks is not unlikely to bring insight into this problem. Additionally our simulation does not model dissociation of the ozone cation, which will play a role in the high energy part of the spectrum.

V. ACKNOWLEDGMENTS

This work was funded by the NSF Center for Chemical Innovation Phase I (grant no. CHE-2221453) and U.S. Department of Energy, Basic Energy Sciences (grant no. DE-FG02-05ER15629).

[1] H. Köppel, W. Domcke, and L.S. Cederbaum, Multimode molecular dynamics beyond the born-oppenheimer approximation, Adv. Chem. Phys. **57**, 59 (1984).

[2] W. Domcke, H. Köppel, and L. S. Cederbaum, Spectroscopic effects of conical intersections of molecular potential energy surfaces, Mol. Phys. **43**, 851 (1981).

[3] H. Köppel, W. Domcke, and L. S. Cederbaum, *The multi-mode vibronic-coupling approach*, chapter 7, pages 323–367. World Scientific Publ Co Pte Ltd, 2004.

[4] R.J. Bartlett and M. Musiał, Coupled-cluster theory in quantum mechanics, Rev. Mod. Phys. **79**, 291 (2007).

[5] A. I. Krylov, Equation-of-motion coupled-cluster methods for open-shell and electronically excited species: The hitchhiker's guide to Fock space, Annu. Rev. Phys. Chem. **59**, 433 (2008).

[6] I. Shavitt and R. J. Bartlett, in *Many-body methods in chemistry and physics: MBPT and coupled-cluster theory*. Cambridge University Press, Cambridge, 2009.

[7] K. Sneskov and O. Christiansen, Excited state coupled cluster methods, WIREs: Comput. Mol. Sci. **2**, 566 (2012).

[8] R. J. Bartlett, Coupled-cluster theory and its equation-of-motion extensions, WIREs: Comput. Mol. Sci. **2**, 126 (2012).

[9] A. I. Krylov, The quantum chemistry of open-shell species, in *Reviews in Comp. Chem.*, edited by A. L. Parrill and K. B. Lipkowitz, volume 30, pages 151–224. J. Wiley & Sons, 2017.

[10] D. A. Matthews and J. F. Stanton, Non-orthogonal spin-adaptation of coupled cluster methods: A new implementation of methods including quadruple excitations, J. Chem. Phys. **142** (2015).

[11] J. F. Stanton and J. Gauss, A simple scheme for the direct calculation of ionization potentials with coupled-cluster theory that exploits established excitation energy methods, J. Chem. Phys. **111**, 8785 (1999).

[12] T. Ichino, J. Gauss, and J. F. Stanton, Quasidiabatic states described by coupled-cluster theory, J. Chem. Phys. **130**, 174105 (2009).

[13] J. Almlöf and P.R. Taylor, General contraction of gaussian basis sets. I. Atomic natural orbitals for first- and second-row atoms, J. Chem. Phys. **86**, 4070 (1987).

[14] J. Almlof, T. Helgaker, and P. R. Taylor, Gaussian Basis Sets for High-Quality ab Initio Calculations, J. Phys. Chem. **92**, 3029 (1988).

[15] D. Woon and T.H. Dunning, Jr., Gaussian basis sets for use in correlated molecular calculations. V. Core-valence basis sets for boron through neon, J. Chem. Phys. **103**, 4572 (1995).

[16] K. A. Peterson and T. H. Dunning, Jr., Accurate correlation consistent basis sets for molecular core-valence correlation effects. the second row atoms Al-Ar, and the first row atoms B-Ne revisited, J. Chem. Phys. **117**, 10548 (2002).

[17] H. Müller, H. Köppel, L. S. Cederbaum, T. Schmelz, G. Chambaud, and P. Rosmus, Vibronic coupling effects in the ozone cation, Chem. Phys. Lett. **197**, 599 (1992).

[18] J.F. Stanton, J. Gauss, M.E. Harding, and P.G. Szalay, CFOUR, with contributions from A.A. Auer, R.J. Bartlett, U. Benedikt, C. Berger, D.E. Bernholdt, Y.J. Bomble, L. Cheng, O. Christiansen, M. Heckert, O. Heun, C. Huber, T.-C. Jagau, D. Jonsson, J. Jusélius, K. Klein, W.J. Lauderdale, F. Lipparini, D.A. Matthews, T. Metzroth, L.A. Mück, D.P. O'Neill, D.R. Price, E. Prochnow, C. Puzzarini, K. Ruud, F. Schiffmann, W. Schwalbach, C. Simmons, S. Stopkowicz, A. Tajti, J. Vázquez, F. Wang, J.D. Watts; and the integral packages MOLECULE (J. Almlöf and P.R. Taylor), PROPS (P.R. Taylor), ABACUS (T. Helgaker, H.J.Aa. Jensen, P. Jørgensen, and J. Olsen), and ECP routines by A.V. Mitin and C. van Wüllen. For the current version, see http://www.cfour.de.

[19] D. A. Matthews, L. Cheng, M. E. Harding, F. Lipparini, S. Stopkowicz, T.-C. Jagau, P. G. Szalay, J. Gauss, and J. F. Stanton, Coupled-cluster techniques for computational chemistry: The CFOUR program package, J. Chem. Phys. **152**, 214108 (2020).

[20] J. M. Dyke, L. Golob, Neville Jonathan, A. Morris, and M. Okuda, Vacuum ultraviolet photoelectron spectroscopy of transient species. Part 4.–Difluoromethylene and ozone, J. Chem. Soc., Faraday Trans. 2 **70**, 1828 (1974).

[21] S. Willitsch, F. Innocenti, J. M. Dyke, and F. Merkt, High-resolution pulsed-field-ionization zero-kinetic-energy photoelectron spectroscopic study of the two lowest electronic states of the ozone cation O_3^+, J. Chem. Phys. **122** (2005).

[22] Riccardo Tarroni and Stuart Carter, Ab initio study of vibronic coupling in the ozone radical cation, Chem. Phys. Lett. **511**, 201 (2011).